


Axial inverse magnetic catalysis

Yuanyuan Wang* and Shinya Matsuzaki†

Center for Theoretical Physics and College of Physics, Jilin University, Changchun 130012, China

 (Received 15 February 2022; accepted 30 March 2022; published 20 April 2022)

We find that the inverse magnetic catalysis (IMC) for $U(1)$ axial symmetry can emerge around the chiral crossover regime in the thermomagnetic QCD with $2 + 1$ flavors at physical point. This phenomenon can be correlated with the IMC for the chiral $SU(2)_L \times SU(2)_R$ symmetry. We explicitly observe the axial inverse magnetic catalysis (AIMC) based on a Nambu-Jona-Lasinio model with $2 + 1$ quark flavors, where introduced anomalous magnetic moments of the quarks play the essential role to drive both the chiral IMC and AIMC. Our finding is shortly testable on lattices. Possible phenomenological and cosmological implications are also briefly addressed.

DOI: [10.1103/PhysRevD.105.074015](https://doi.org/10.1103/PhysRevD.105.074015)

I. INTRODUCTION

Violation of $U(1)$ axial symmetry plays a key role to address the QCD vacuum characterized by quark condensates, as well as the chiral symmetry breaking. In particular, it has been a longstanding issue how much the $U(1)_A$ breaking contributes to the quark condensate. This question could be related to what is the major role for the origin of mass in the thermal history of the Universe.

The state-of-art-lattice simulations have so far clarified that in the hot QCD with $2 + 1$ (light up and down quarks and one heavy strange quark), the $U(1)_A$ axial breaking tends to survive longer than the chiral $SU(2)$ breaking for the lightest two flavors as temperature grows [1,2]. This result is also supported from a rigorous argument based on QCD-inequality-like relations [3] and its generalized evidence based on the lattice QCD setup [4]. Moreover, a recent lattice study (with two lightest flavors) has shown a hint that significantly dominant contributions from the $U(1)_A$ breaking are left in the quark condensate, during the chiral phase transition (crossover) [5]. All those may imply that in a view of the thermal history of the Universe, the main source for the origin of mass is supplied from the $U(1)_A$ breaking.

However, it might be not the end of the story: even in early Universe including the QCD phase transition epoch, a strong enough magnetic field might be present as a background field, which could be generated due to some

primordial (electroweak) phase transitions of strong first order [6–12]. Therefore, the QCD dynamics in the thermal history might be thermomagnetic, which is called thermomagnetic QCD. In addition, heavy ion collision experiments [13–20] can create a strong enough magnetic field in the thermal plasma of QCD, due to the relativistic motion of the colliding nuclei and the smallness of the system. Thus, the thermomagnetic QCD has nowadays opened a vast ballpark, not only with cosmological, but also experimental interests, involving lattice simulations, and chiral-effective model approaches.

Some outstanding results have already been reported from lattice studies on the QCD thermodynamics in a strong external magnetic field [21,22]. Of particular importance related to the chiral symmetry breaking are the reduction of the pseudocritical temperature for the chiral crossover [23–27] and the inverse magnetic catalysis [28]. Both two imply a faster effective restoration of the chiral symmetry in hot-magnetized early Universe. To our best knowledge, however, no definite analysis on the $U(1)_A$ breaking and effective restoration in the thermomagnetic QCD has been carried out, or no implications of the inverse magnetic catalysis for the chiral symmetry to the $U(1)_A$ symmetry have been argued.

In this paper, prior to lattice simulations in the near future, based on a chiral effective model we observe a definite implication of the inverse magnetic catalysis for the chiral symmetry, to the $U(1)_A$ breaking in thermomagnetized QCD: that is the inverse magnetic catalysis (IMC) for the $U(1)_A$ symmetry, which we call the axial IMC (AIMC), and in comparison, we call the IMC for the chiral $SU(2)_L \times SU(2)_R$ symmetry CIMC. We employ a Nambu-Jona-Lasinio (NJL) model with $2 + 1$ flavors at the physical point, in which we introduce a couple of anomalous magnetic moments (AMMs) of quarks, as well as so-called Kobayashi-Maskawa-’t Hooft determinant term [29–32]

*yuanyuanw20@mails.jlu.edu.cn

†synya@jlu.edu.cn

Published by the American Physical Society under the terms of the [Creative Commons Attribution 4.0 International license](https://creativecommons.org/licenses/by/4.0/). Further distribution of this work must maintain attribution to the author(s) and the published article’s title, journal citation, and DOI. Funded by SCOAP³.

mimicked as the instanton-induced $U(1)_A$ anomaly in the underlying QCD.

We first look into the viable parameter space to realize the CIMC, which is mapped on the AMM parameters. Then we evaluate the difference of susceptibilities for the $U(1)_A$ partner, such as π and δ mesons, denoted as χ_π and χ_δ as a function of the applied constant magnetic field and temperature. In terms of the axial susceptibility, $\chi_{\pi-\delta} \equiv \chi_\pi - \chi_\delta$, the AIMC is dictated by observing that at zero temperature, $\chi_{\pi-\delta}$ becomes larger and larger, as the magnetic field strength increases, and the pseudocritical temperature of $\chi_{\pi-\delta}$, T_{pc}^A , gets smaller as the magnetic field gets stronger. Here T_{pc}^A is defined as the inflection point of the temperature evolution of $\chi_{\pi-\delta}$.

In light of the CIMC, the two-flavor NJL model with AMMs of quarks has so far been discussed [33–39]. There, in terms of the symmetry argument, realization of the CIMC can be understood by emergence of destructive interference in the light-quark condensates between two explicit chiral-breaking sources, where one comes from the current quark mass, while the other from the AMMs of quarks coupled to a strong magnetic field. No explicit work on the chiral phase transition has been done with $2 + 1$ flavors coupled with the AMMs in the framework of NJL.

We will shed the first light on the $2 + 1$ flavor case, and clarify the fully viable parameter space to realize the desired CIMC at high temperatures, and MC at zero temperature. We find that at any temperature including zero temperature, the AMMs of u and d quarks contribute to the u and d quark condensates, or the constituent- u and d quark masses, destructively against effects from the current quark mass and the $U(1)_A$ anomaly, while the AMM of strange quark acts as destructive interference at lower temperature, and constructive one at higher temperatures: namely, the AMM of strange quark tends to cease realization of MC and CIMC, at zero temperature and higher temperatures, respectively. This latter feature is a new finding characteristic to the $2 + 1$ flavor model.

Since the AMM interactions break not merely the chiral $SU(2)_L \times SU(2)_R$ symmetry, but the $U(1)_A$ symmetry, similar destructive interference is expected to happen in the $U(1)_A$ sector, i.e., $\chi_{\pi-\delta}$. Such coincidental correlation between the chiral and $U(1)_A$ symmetries may also be deduced in a context of the QCD-inequality argument [1,3], and a recent lattice study detailed on the Dirac spectrum [40,41]. The latter, in particular, works through an operator identitylike relation between the Dirac spectrum, the chiral condensate, and the $U(1)_A$ susceptibility, and should hold even including external fields, such as a constant magnetic field. Still, however, it would be nontrivial in a sense of framework of chiral effective models to monitor such chiral- $U(1)_A$ axial coherence in the $2 + 1$ flavor case. Based on the NJL model with AMMs, we will explicitly clarify how efficiently the destructive interference arises in the $U(1)_A$ susceptibility $\chi_{\pi-\delta}$, coherently in the chiral condensate.

We find that the AIMC can take place in the chiral crossover regime where the CIMC is present, which depends on the size of AMM, and the pseudocritical temperature T_{pc}^A drops as the magnetic field strength increases. Lattice simulations in the near future will give a decisive conclusion on existence of the AIMC and the competition for the survival between the chiral and $U(1)_A$ breaking at higher temperatures.

This AIMC may provide a hint to reveal whether in a sense of early thermomagnetic universe, the remnant of the $U(1)_A$ breaking in the origin of mass might be comparable with what the chiral breaking leaves, in contrast to the pure-thermal QCD in which the former might highly dominate [5].

Other phenomenological and cosmological implications deduced from the AIMC are also briefly addressed.

II. NJL MODEL WITH QUARK AMM: PRELIMINARIES

To clarify the presence of AIMC, we work on a NJL model with $2 + 1$ flavors with AMMs of quarks in a constant magnetic field. The model is described by the following Lagrangian:

$$\begin{aligned} \mathcal{L} = & \sum_{f=u,d,s} \bar{\psi}_f (i\gamma^\mu D_\mu^{(f)} - \hat{m}_{0f} + \kappa_f(eB, T) q_f F_{\mu\nu} \sigma^{\mu\nu}) \psi_f \\ & + G \{ (\bar{\psi} \lambda^a \psi)^2 + (\bar{\psi} i\gamma^5 \lambda^a \psi)^2 \} \\ & - K [\det \bar{\psi} (1 + \gamma_5) \psi + \det \bar{\psi} (1 - \gamma_5) \psi]. \end{aligned} \quad (1)$$

Here $\psi_f = (u, d, s)^T$ denotes the three-flavor quark field forming the $SU(3)$ triplet; for simplicity, the current-quark mass matrix \hat{m}_{0f} is taken to be diagonal in the flavor space: $\hat{m}_{0f} = \text{diag}(m_{0u}, m_{0d}, m_{0s})$, where the present $2 + 1$ flavor setup leads to $m_{0u} = m_{0d} \equiv m_0$; λ^a ($a = 0, \dots, 8$) are the Gell-Mann matrices in the flavor space with $\lambda^0 = \sqrt{2/3} \text{diag}(1, 1, 1)$; the covariant derivative $D_\mu^{(f)} = \partial_\mu - iq_f A_\mu$ contains the coupling between the quark and the external magnetic field with the electromagnetic charge matrix $q_f = e \cdot \text{diag}\{2/3, -1/3, -1/3\}$, where the magnetic field is applied along the z direction and embedded in the electromagnetic gauge field A_μ as $A_\mu = (0, 0, Bx, 0)$; $F_{\mu\nu} = \partial_\mu A_\nu - \partial_\nu A_\mu$ is the electromagnetic field strength; G and K are the four-fermion coupling constant and the determinant (six-fermion) coupling constant, respectively; $\sigma^{\mu\nu} = \frac{i}{2} [\gamma^\mu, \gamma^\nu]$. The $\kappa_f(eB, T)$ is the AMM coupling, which is related to the AMM for quark a_f as $a_f = 4M_f \cdot \kappa_f$ with the constituent quark mass M_f . Here κ_f itself is dependent of quark flavors, the background temperature T , and an applied strong enough magnetic field B , to be fixed later [see Eq. (10)].

Under the chiral $U(3)_L \times U(3)_R$ transformation: $\psi \rightarrow U \cdot \psi$ with $U = \exp[-i\gamma_5 \sum_{a=0}^8 (\lambda^a/2) \theta^a]$ and the

chiral phases θ^a , the four-fermion interaction term is $U(3)_L \times U(3)_R$ invariant. The mass term explicitly breaks the chiral $U(3)_L \times U(3)_R$ symmetry. The determinant term, called Kobayashi-Maskawa-'t Hooft (KMT) determinant [29–32], is induced from the instanton coupled to quarks in the underlying QCD, and preserves the chiral $SU(3)_L \times SU(3)_R$ invariance (associated with the chiral phases labeled as $a = 1, \dots, 8$), but breaks the $U(1)_A$ (corresponding to $a = 0$) symmetry. The AMM term with the coupling κ_f explicitly breaks not only the chiral $SU(3)_L \times SU(3)_R$ symmetry, but also the $U(1)_A$ axial symmetry.

In addition to the quark mass terms, the KMT determinant term, and the AMM term, the chiral $U(3)_L \times U(3)_R$ symmetry is spontaneously broken by the nonperturbative dynamics of the present NJL. To monitor the spontaneous breaking, we simply employ the mean-field approximation, and construct the thermodynamic potential in the presence of a constant magnetic field. The thermodynamic potential is then given as a function of thermally averaged quark condensates; $\langle \bar{u}u \rangle$, $\langle \bar{d}d \rangle$, and $\langle \bar{s}s \rangle$, are determined via the stationary condition of the potential, i.e., the gap equations: $\langle \bar{f}f \rangle = -iN_c \text{tr} \int \frac{d^4 p}{(2\pi)^4} S^f(p)$, where $S^f(p)$ stands for the full propagator of f quark and N_c is the number of colors, to be fixed to three. With respect to those quark condensates, the thermodynamic potential is minimized at the nontrivial vacuum with the stationary condition. We then find the coupled gap equations in terms of the constituent quark masses $M_f = (M_u, M_d, M_s)$, which take the same form as in the case without the magnetic field [42]:

$$M_f = m_{0f} + \sigma_f, \quad (2)$$

where

$$D_n(q_f B, p) = (p^0 \gamma^0 - p^3 \gamma^3 + M_f + \kappa_f q_f B \sigma^{12}) \left[(1 + i\gamma^1 \gamma^2 \text{sign}(q_f B)) L_n \left(\frac{2\vec{p}_\perp^2}{|q_f B|} \right) - (1 - i\gamma^1 \gamma^2 \text{sign}(q_f B)) L_{n-1} \left(\frac{2\vec{p}_\perp^2}{|q_f B|} \right) \right] + 4(p^1 \gamma^1 + p^2 \gamma^2) L_{n-1}^1 \left(\frac{2\vec{p}_\perp^2}{|q_f B|} \right), \quad (6)$$

$$F_n(q_f B, p) = (\kappa_f q_f B - p^0 \gamma^3 \gamma^5 + p^3 \gamma^0 \gamma^5)^2 - M_f^2 - 2n|q_f B|, \quad (7)$$

$$A_n(q_f B, p) = [(\kappa_f q_f B + \sqrt{p_\parallel^2})^2 - M_f^2 - 2n|q_f B|] \times [(\kappa_f q_f B - \sqrt{p_\parallel^2})^2 - M_f^2 - 2n|q_f B|], \quad (8)$$

with $p_\parallel^2 = p_0^2 - p_3^2$.

¹Here L_n^α denotes the generalized Laguerre polynomials.

$$\begin{aligned} \sigma_u &= 4iG \langle \bar{u}u \rangle - 2K \langle \bar{d}d \rangle \langle \bar{s}s \rangle, \\ \sigma_d &= 4iG \langle \bar{d}d \rangle - 2K \langle \bar{u}u \rangle \langle \bar{s}s \rangle, \\ \sigma_s &= 4iG \langle \bar{s}s \rangle - 2K \langle \bar{u}u \rangle \langle \bar{d}d \rangle. \end{aligned} \quad (3)$$

In evaluating the thermally averaged quark condensates, we apply the imaginary time formalism. Taking into account nonzero constant magnetic field applied along the z direction as well, we shall make the following replacements:

$$\begin{aligned} p_0 &\rightarrow i\omega_{\mathbf{k}} = i(2\mathbf{k} + 1)\pi T, \\ \int \frac{d^4 p}{(2\pi)^4} &\rightarrow iT \sum_{\mathbf{k}=-\infty}^{\infty} \int \frac{d^3 p}{(2\pi)^3} \\ &\rightarrow iT \sum_{\mathbf{k}=-\infty}^{\infty} \sum_{f=u,d,s} \sum_{n=-\infty}^{\infty} \frac{|q_f B|}{2\pi} \int_{-\infty}^{\infty} \frac{dp_3}{2\pi}, \end{aligned} \quad (4)$$

with the Matsubara frequency $\omega_{\mathbf{k}}$ and the Landau level n . Thus the analysis will be straightforward just by extending the one in the literature [42] to the case with the magnetic field and AMMs.

The f -quark propagator $S^f(p)$ including the AMM term is available in the literature [38], which takes the form

$$S^f(p) = ie^{-\frac{\vec{p}_\perp^2}{|q_f B|}} \sum_{n=0}^{\infty} \frac{D_n(q_f B, p) F_n(q_f B, p)}{A_n(q_f B, p)}, \quad (5)$$

where $p_\perp = (p_1, p_2)$, and¹

To regularize the intrinsic divergence terms arising in the momentum integration along the magnetic field direction (p_3), we adopt a smooth cutoff scheme with the cutoff function,

$$f_\Lambda(p_3, n) = \frac{\Lambda^{10}}{\Lambda^{10} + (p_3^2 + 2n|q_f B|)^2}, \quad (9)$$

where Λ is the cutoff for the three-dimensional momentum integral in Eq. (4).

The AMM term breaks the full $U(3)_L \times U(3)_R$ symmetry even at the classical or perturbative level of QED. In a strong enough magnetic field, moreover, the AMM can actually be dynamically developed [33,43–48] as another

chiral order parameter, simultaneously with the quark condensates. This dynamical generation would happen when the scale of the magnetic field strength would be comparable with or greater than the intrinsic infrared scale of QCD or the NJL dynamics, say the renormalization-group invariant Λ_{QCD} , or (equivalently) dynamical quark mass at vacuum (~ 300 MeV). Such strong enough magnetic field would cause the dimensional reduction: $D = 4 \Rightarrow 2$ with the reduced Lorentz symmetry left in $D = 2$: $SO(1, 3) \Rightarrow SO(1, 1) \times O(2)$, in which both the dynamics and kinematics are separately characterized by spaces parallel (\parallel) and transverse (\perp) to the applied magnetic field direction (the z direction). This is how the AMM operator $\bar{q}_f \sigma_{12} q_f$ would be allowed to condense in the residual- $SO(1, 1) \times O(2)$ invariant way, to contribute to the dynamical chiral symmetry breaking, together with the normal quark condensate operator $\bar{q}_f q_f$, as has been discussed in the literature [33,43–48].

In the present analysis, we assume the dynamical AMM to dominate over the perturbative contribution generated at the leading order of QED. Then, the AMM should be related to the dynamical mass part of the constituent quark mass. Inspired by the dynamical AMM generation via the NJL dynamics as in the literature listed above, but, still allowing the AMMs as free parameters,² we may model the relation between the AMMs (κ_f) and the dynamical mass parts of the quarks [σ_f in Eq. (2)] as³

$$\kappa_f(eB, T) = v_f \cdot \sigma_f(eB, T), \quad \text{for } eB \gtrsim eB|_{\min}, \quad (10)$$

with the lower bound of the magnetic field strength, $\sqrt{eB}|_{\min}$, which is to be fixed later. The flavor-dependent coefficient v_f is assumed to be flavor universal for u and d quarks, i.e., $v_u = v_d \equiv v$, but is taken to be different for s quark: $v_s \neq v$. This would be a reasonable setup because the AMM parameter κ_f is defined exclusively out of the overall electromagnetic charge, as seen from Eq. (1), and QCD (or NJL dynamics) is potentially flavor universal, hence the discrepancy in AMMs among flavors arises only from the chiral-explicit breaking sources, which can be fully incorporated in the dynamical mass part σ_f .

²We have checked that the size of the NJL-driven AMM is too small to realize the CIMC at higher T . In this sense, it is necessary to go beyond the one-gluon exchange prescription of the NJL for the AMM. Note, however, that as long as we work on the leading order of the large N_c expansion (or mean-field approximation), even NJL-driven AMM term can be reduced to the κ_f term in Eq. (1). Therefore, we can interpret the size of v and v_s as displayed in the plots later as the net contribution from the NJL-driven and beyond NJL effects.

³A similar procedure has been applied in Ref. [38] for the 2-flavor NJL case, with $v_u = v_d$ assumed.

In closing this preliminary section, we introduce five model parameters fixed at vacuum with $eB = T = 0$: $m_0 = 0.0055$ GeV, $m_{0s} = 0.1407$ GeV, $\Lambda = 0.6023$ GeV, $G\Lambda^2 = 1.835$, and $K\Lambda^5 = 12.36$, which are quoted from the literature [42], where inputs are an optimized and conventional set of the hadronic observables in the isospin-symmetric limit: $m_\pi = 0.135$ GeV, $m_K = 0.4977$ GeV, $m_{\eta'} = 0.9578$ GeV, $f_\pi = 0.0924$ GeV, and $m_0 = 5.5$ MeV.

We will not consider intrinsic-temperature dependent couplings, instead, all the T dependence should be induced only from the thermal quark loop corrections to the couplings defined and introduced at vacuum. Actually, the present NJL at $eB = 0$ shows good agreement with lattice QCD results on the temperature scaling for the chiral, axial, and topological susceptibilities, as shown in Ref. [49]. In this sense, we do not need to introduce such an intrinsic T dependence for the model parameters in the regime up to temperatures around the chiral crossover.

III. CIMC AND “PHASE” DIAGRAM

With the preliminary setup provided in the previous section, we first evaluate the constituent quark mass for u and d quarks as a function of temperature T , given the strength of the applied magnetic field and the AMM parameters v and v_s . See Fig. 1. We have taken $\sqrt{eB} \sim (0.5\text{--}0.6)$ GeV for a wide range of T , (0.05–0.25) GeV, where the strength of magnetic field is strong enough in light of lattice QCD: the constant magnetic field applied on lattice QCD has the minimal size fixed as $|eB|_{\min} \propto T^2$ [28], and one can check that $\sqrt{eB}|_{\min} < T_{\text{highest}} \sim 0.25$ GeV $< \sqrt{eB}|_{\text{applied}} \sim (0.5\text{--}0.6)$ GeV. In the figure, we have plotted the averaged mass for u and d quarks, $M = \frac{M_u + M_d}{2}$, which is a reasonable chiral order parameter in the presence of a couple of isospin breaking sources, and

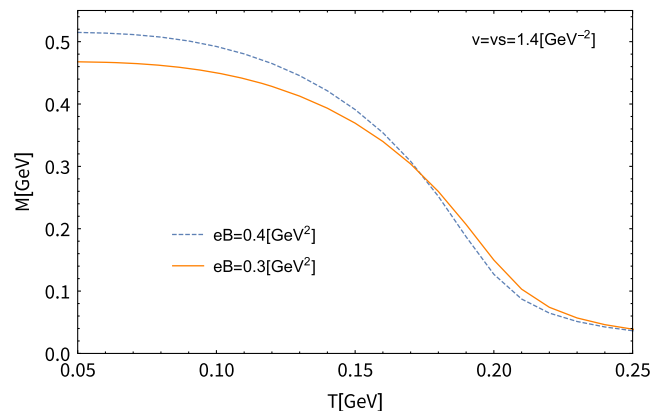


FIG. 1. Plot of the averaged constituent mass for u and d quarks, M , versus temperature evolution, with eB varied and the AMM parameters v and v_s being fixed to a reference point (included in the allowed regime of the “phase” diagram in Fig. 2).

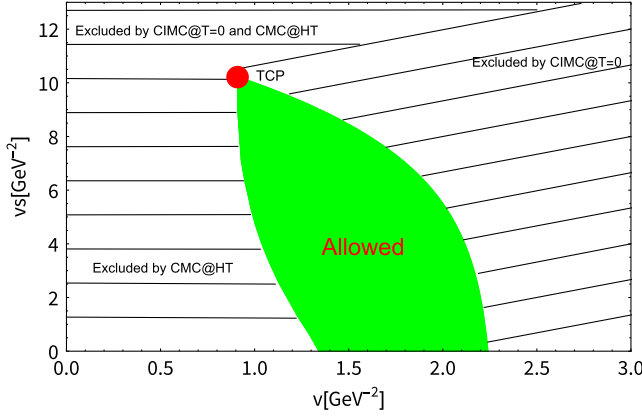


FIG. 2. The phase diagram on (v, v_s) plane classified by the CMC and CIMC features at $T = 0$ and higher temperatures (HT). The three phases filled by shaded lines, corresponding to [1], [2] and [3] in the text, are ruled out because of failure of realizing the magnetic features on the chiral symmetry breaking, reported from lattice QCD. Only the centered regime of green-leaf shape is allowed. All the four phases merge at the tetra-critical point, TCP, denoted as a blob.

taken the AMM parameters $v = v_s = 1.4 \text{ GeV}^{-2}$, as a reference point to be clarified below. We see that for small T , M increases as the magnetic field gets larger, while at higher T , it turns to decrease with the magnetic field. This confirms the CIMC phenomenon, and is a successful result generalized from the two-flavor NJL with the AMM [33–39], to the 2 + 1 flavor case including the KMT-determinant $U(1)_A$ -anomaly contribution [K terms in Eq. (3)]. The CIMC is successfully realized essentially due to a moderately large AMM for u and d quarks which constructively contributes to M with the thermal corrections, to make M dropped faster.

Scanning over the AMM parameter space (v, v_s) with the size of eB varied in an appropriately strong enough range (as noted above), we examine the MC and IMC features at $T = 0$ and at higher T . Thus, the phase diagram is drawn on the (v, v_s) space, as depicted in Fig. 2. The diagram turns out to be divided into four phases, where the model realizes

- [1] CIMC for any T including $T = 0$, due to larger AMMs for u and d quarks;
- [2]] CMC for any T including $T = 0$, due to smaller AMM for u and d quarks;
- [3] CIMC at $T = 0$, and CMC at higher temperatures, due to significant AMM for strange quark;
- [4] CMC at $T = 0$, and CIMC at higher temperatures, due to moderate AMMs for 2 + 1 quarks.

The first three phases [1], [2], and [3] are excluded, because they do not reproduce the lattice results on the CMC and CIMC. Thus, only the phase [4] survives, which corresponds to the “Allowed” regime in Fig. 2. One may notice that there is a critical point at which all four phases merge

on the diagram, that is, the tetra-critical point (TCP), which has been also specified in Fig. 2.

Of particular interest is to note the phase [3], where the AMM of strange quark acts like a destructive interference against realization of the CMC at $T = 0$ and CIMC at higher temperatures. This is in contrast to the role of the AMM for u and d quarks. It is operative in the light-quark constituent mass (M), and contributes destructively against the current quark mass and the $U(1)_A$ anomaly at any temperature including zero temperature, so that when it is too large, the CIMC is driven even at $T = 0$ (phase 1), while the CMC shows up at any temperature, when the light-quark AMM is too small (phase 2). This feature can also be observed by viewing the plot along the v axis at $v_s = 0$, in Fig. 2.

With the phase diagram taken into account, below we will discuss the T and eB dependence on the axial susceptibility.

IV. AXIAL SUSCEPTIBILITY: $\chi_{\pi-\delta}$, AMC, AND AIMC

The axial susceptibility is constructed from difference of two susceptibilities related to the $U(1)_A$ partners. In the present NJL model with 2 + 1 flavors, we have two candidates of the $U(1)_A$ partners, which are, in terms of meson names, (σ, η) and (π, δ) . Those cases should be just alternatives of each other, and exhibit the same axial property, which would be so even at finite T and eB . In the present analysis, we take π and δ meson channels, and investigation of the other partner is to be pursued in another publication.

We start with evaluating the π channel. The π meson susceptibility χ_π is defined as

$$\chi_\pi = \int_T d^4x [\langle (\bar{u}(0)i\gamma_5 u(0))(\bar{u}(x)i\gamma_5 u(x)) \rangle_{\text{conn}} + \langle (\bar{d}(0)i\gamma_5 d(0))(\bar{d}(x)i\gamma_5 d(x)) \rangle_{\text{conn}}], \quad (11)$$

with $\langle \dots \rangle_{\text{conn}}$ being the connected part of the correlation function. Here the spacetime integral with the subscript symbol T means $\int_0^{\beta=1/T} d\tau \int d^3x$, reflecting the currently employed imaginary time formalism. Following the literature [50], the explicit formula for χ_π in the present NJL model reads

$$\chi_\pi = \frac{\Pi_\pi(0, 0)}{1 - [2G - K\langle \bar{s}s \rangle]\Pi_\pi(0, 0)}, \quad (12)$$

with $\Pi_\pi(0, 0) \equiv \Pi_\pi(\omega, \vec{p})$ being the polarization (correlation) function for the π channel. Presently, we focus only on the neutral meson channel, so that $\Pi_\pi(0, 0)$ is evaluated as

$$\Pi_\pi(0,0) = -i \cdot \sum_{f=u,d} \left(\int \frac{d^4 p}{(2\pi)^4} \text{tr}[i\gamma_5 S^f(p) i\gamma_5 S^f(p)] \right). \quad (13)$$

Similarly, we next evaluate the δ meson susceptibility, which is defined as

$$\chi_\delta = \int_T d^4 x \left[\langle (\bar{u}(0)u(0))(\bar{u}(x)u(x)) \rangle_{\text{conn}} + \langle (\bar{d}(0)d(0))(\bar{d}(x)d(x)) \rangle_{\text{conn}} \right]. \quad (14)$$

The explicit formula for χ_δ reads [50]

$$\chi_\delta = \frac{\Pi_\delta(0,0)}{1 - [2G + K\langle \bar{s}s \rangle] \Pi_\delta(0,0)}. \quad (15)$$

Focusing on the neutral δ meson component, we find the corresponding polarization function in the δ^0 meson channel:

$$\Pi_\delta(0,0) = -i \cdot \sum_{f=u,d} \left(\int \frac{d^4 p}{(2\pi)^4} \text{tr}[S^f(p)S^f(p)] \right). \quad (16)$$

The more detailed expressions for Π_δ as well as Π_π are presented in the Appendix, which are useful for performing numerical analysis.

It is crucial to note that χ_π is related to the light-quark condensates, through the chiral Ward identity [51–53] as

$$\langle \bar{u}u \rangle + \langle \bar{d}d \rangle = -m_0 \chi_\pi. \quad (17)$$

This is operative even at finite temperature [53], and can also work even with a constant magnetic field, though it provides extra explicit-chiral/isospin breaking term. The recent lattice 2 + 1 flavor simulation [54] has also proved that when $m_u = m_d$, Eq. (17) indeed holds in the magnetic field for each of u and d terms at the operator level, so it should work also at any temperature. Indeed, we have checked that Eq. (17) is satisfied with χ_π and light-quark condensates.

Making difference of χ_π and χ_δ , we define the axial susceptibility as

$$\chi_{\pi-\delta} \equiv \chi_\pi - \chi_\delta. \quad (18)$$

This $\chi_{\pi-\delta}$ becomes zero, when the $U(1)_A$ symmetry is exact, because $\chi_\pi \leftrightarrow \chi_\delta$ by the $U(1)_A$ transformation, as is manifest in the definitions, Eqs. (11) and (14). In Fig. 3 we plot the magnitude of $\chi_{\pi-\delta}$ as a function of eB at $T = 0$, with the AMM values fixed inside (for $v = v_s = 1.4 \text{ GeV}^{-2}$) or outside (for $v = v_s = 0$) the allowed regime in the phase diagram, Fig. 2. We observe that $|\chi_{\pi-\delta}|$ gets larger as eB grows, namely, the MC for the axial symmetry at $T = 0$. Realization of the AMC at $T = 0$ is somewhat

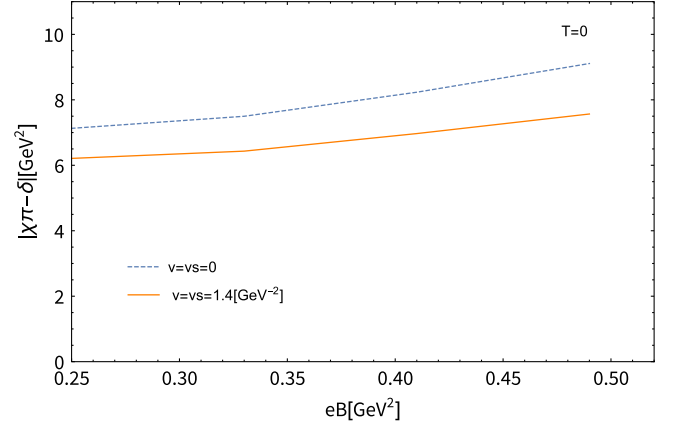


FIG. 3. The magnitude of the axial susceptibility, $|\chi_{\pi-\delta}|$, versus the strength of eB , at zero temperature, with a couple of reference AMM values inside and outside the Allowed regime in Fig. 2. Both cases realize the AMC. The size of eB has been bounded from below, at $eB \geq 0.25 \text{ GeV}^2$, which is to be consistent with quantitative agreement of the present NJL model on the eB dependence of the subtracted quark condensates at $T = 0$ with those reported from lattice QCD. For details, see the Summary and Discussion section and Fig. 8.

insensitive to the size of the AMMs, in sharp contrast to the case of the CMC at $T = 0$.

From Fig. 4, we also notice the trend of monotonic reduction for the magnitude by finite AMMs, with fixed eB , which is observed irrespective to v or v_s . This is because all the AMMs play a destructive interference in $\chi_{\pi-\delta}$, against contributions from the current quark masses and the KMT-determinant $U(1)_A$ anomaly, to drive faster $U(1)_A$ restoration.

This trend is observed even at finite temperature. See Fig. 4, which shows $|\chi_{\pi-\delta}|$ as a function of T , with eB fixed and the sizes of the AMMs being flavor symmetrically ($v = v_s$) or asymmetrically ($v \neq v_s$) varied. Larger AMMs tend to reduce the magnitude of $|\chi_{\pi-\delta}|$ at any temperature, and the AMMs generically play a role of catalyzer toward the $U(1)_A$ symmetry restoration.

Figure 5 shows the T dependence of $|\chi_{\pi-\delta}|$ with eB varied, at a reference allowed point for the AMMs (v, v_s) in Fig. 2. We see that $|\chi_{\pi-\delta}|$ starts to drop faster at higher temperatures, as eB gets larger, while it develops with eB at lower temperatures. This implies the IMC for the $U(1)_A$ symmetry, i.e., AIMC, in perfect analogy to the IMC for the chiral symmetry (CIMC). This AIMC can further be quantified by observing the eB dependence on the pseudocritical temperature, T_{pc}^A , which is defined as the inflection point of the $|\chi_{\pi-\delta}|$ curve with respect to T as

$$\left. \frac{\partial^2 |\chi_{\pi-\delta}|}{\partial T^2} \right|_{T=T_{pc}^A} = 0. \quad (19)$$

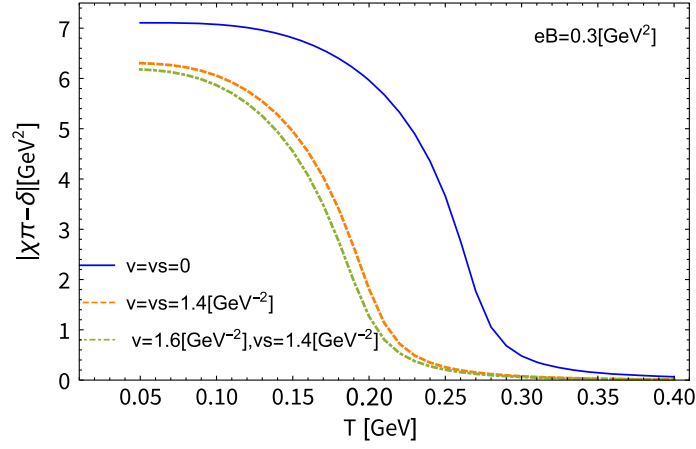


FIG. 4. The AMM dependence on $|\chi_{\pi-\delta}|$ at finite temperature, with eB fixed.

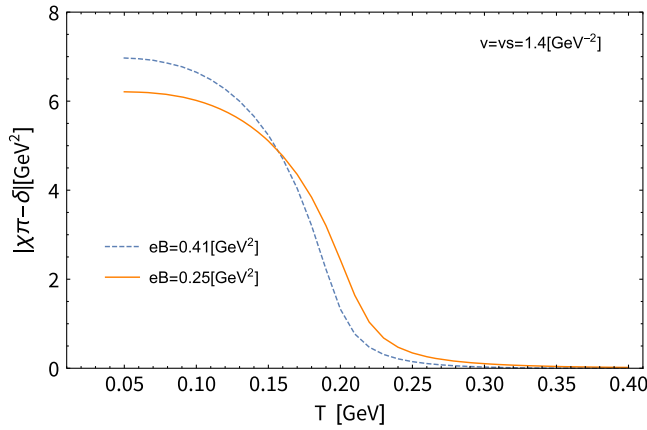


FIG. 5. Plots of $|\chi_{\pi-\delta}|$ as a function of T , with eB varied, at a viable reference point for the AMMS (v, v_s) in the phase diagram, Fig. 2. The AIMC is observed.

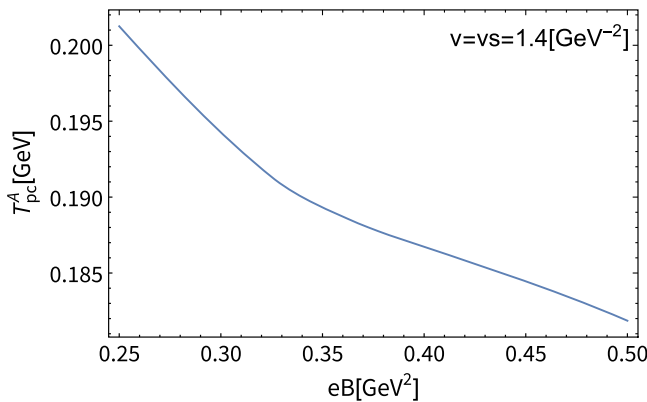


FIG. 6. The eB scaling of the pseudocritical temperature for $|\chi_{\pi-\delta}|$, T_{pc}^A defined in the text. The AMM values have been set to the same viable reference point as in Fig. 5. The observed decreasing trend manifests presence of the AIMC. The range of eB has been restricted to be ≥ 0.25 GeV^2 , for the same reason as noted in the caption of Fig. 3.

Figure 6 plots this T_{pc}^A as a function of eB , at the same reference point for AMMS as in Fig. 5. A monotonic decrease trend for T_{pc}^A with growing eB is indeed observed, so it manifests the AIMC, just like the case of the CIMC.

Finally, in Fig. 7 we show an extended phase diagram on the AMM (v, v_s) plane of Fig. 2, by incorporating the parameter space to realize the AIMC at high temperatures. The figure tells us that the AIMC at high temperature is necessarily realized when the desired CMC at lower T and the CIMC at higher T are present (filled in green), except for domains with a larger AMM for strange quark (in

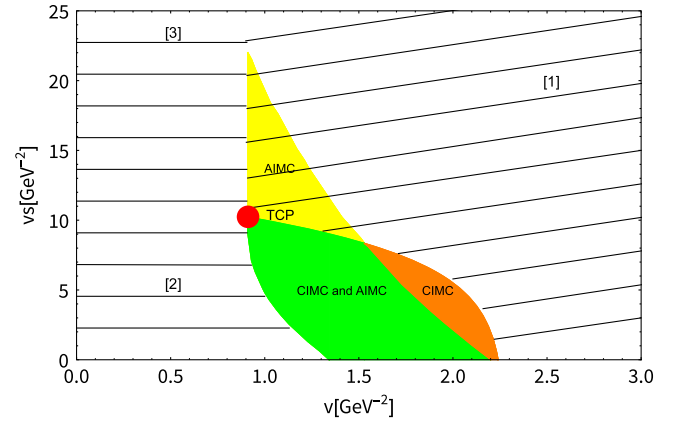


FIG. 7. The phase diagram extended from Fig. 2 with the property of the axial sector incorporated. In the same way as in Fig. 2, the phase [1] is excluded by CIMC at $T = 0$; [2] is ruled out by CMC at higher temperatures; [3] is disfavored because of CIMC at $T = 0$ and CMC at higher temperatures. The TCP is placed at the same point as in Fig. 2. The domain filled in yellow, which realizes the AIMC at higher temperatures, almost overlaps with the Allowed regime in Fig. 2, but separates into two, to create the orange regime out of the original green Allowed regime. The reason would be related to the calculability of the present analysis. For more details, see the text.

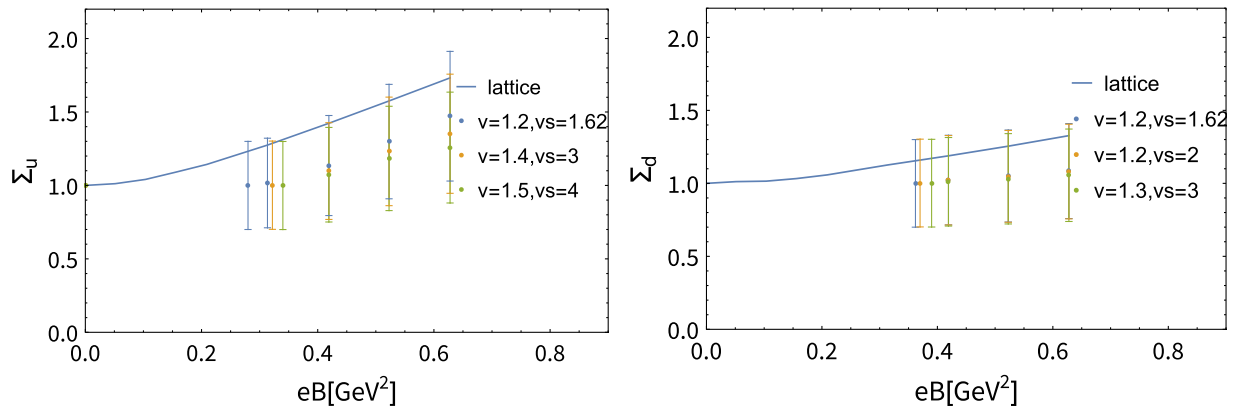


FIG. 8. Comparison of eB dependence on the subtracted quark condensates Σ_u (left panel) and Σ_d (right panel) at $T = 0$, with the $2 + 1$ flavor lattice data (solid curve) [54]. Error bars along with the model yields correspond to the 30% uncertainty, described in the text. The values of v and v_s are read with unit of GeV^{-2} .

yellow) including the TCP (red blob), or with a larger AMM for up and down quarks (in orange).

The former discrepancy is due to the flavor-universal destructive contribution from the AMMs to $|\chi_{\pi-\delta}|$, hence even so large v_s can still act as a destructive interference in $|\chi_{\pi-\delta}|$ against the other axial breaking contributions from the current quark mass and $U(1)_A$ anomaly. This feature is contrast to the v_s sensitivity to the chiral symmetry, as emphasized above, for which the property of the v_s interference changes in low or high temperatures.

The latter case would involve limitation of the present analysis based on the NJL description. The boundary separating the “CIMC and AIMC” (in green) and “CIMC” (in orange) domains has been created by the present calculability: going over the CIMC and AIMC domain to the right (i.e., to a larger v regime) $|\chi_{\pi-\delta}|$ actually starts to show nonmonotonic damping scaling at higher T , which we would regard as unphysical or an artifact of the present NJL model as a low energy description of QCD. This lack of calculability has also affected the existence of a top endpoint of the AIMC regime [at $(v, v_s) \simeq (0.9, 22)$], and the right-side boundary curve in Fig. 7.

The left-side lower boundary curve (green part) is present because the AMC at higher temperatures is realized due to too small AMMs, which corresponds to the phase [2], while the upper boundary curve (yellow part) has been created because of lack of calculability due to too large v_s , similarly to the aforementioned case with too large v .

Lattice simulations in the near future will clarify the AIMC, and give a conclusive answer to whether the AIMC at high temperatures is necessarily realized when the CIMC at high temperatures is present.

V. SUMMARY AND DISCUSSION

We found the AIMC at high temperatures, which can be driven by the $2 + 1$ flavor-universal destructive interference against the current quark mass and the $U(1)_A$ anomaly in the axial susceptibility, when the CIMC is present. One possible candidate to realize this kind of destructive effects involves the AMMs of quarks, which, in the present paper, we have incorporated into a NJL model with $2 + 1$ flavors, to observe emergence of the AIMC at the physical point. Measuring the AIMC would give a complementary probe of the CIMC (See Fig. 6), and imply a definite interpretation on how the IMC is realized: it is due to the destructive axial- and chiral-breaking driven in thermomagnetic QCD. Our findings are shortly testable by lattice simulations in the near future, by which the AMM values in the NJL model can be constrained and a part of the model parameter space will be excluded or probed.

Several comments are in order.

- (i) The presence of the AIMC manifests the intrinsic and nonfactorizable chiral-axial correlation, which has been supported from a recent rigorous proof by the lattice study [40]. This correlation can be suspected also from the result in [49] at zero magnetic field, based on the same NJL model with $2 + 1$ flavors as in the present paper, which is tightly constrained by single anomalous-chiral Ward identity involving the chiral and axial susceptibilities, together with the topological susceptibility.
- (ii) Though both emergence of the CIMC and AIMC are qualitatively interpreted by presence of AMM parameters for quarks and its destructive interference against the current quark mass and axial anomaly effects, we may check its quantitative consistency of the presence of such sizable parameters, by

evaluating the eB dependence of the subtracted light-quark condensate $\Sigma_f \equiv 1 + \frac{2m_{0f}}{m_{\pi}^2 f_{\pi}^2} (\langle -\bar{q}_f q_f \rangle (eB \neq 0) - \langle -\bar{q}_f q_f \rangle (eB = 0))$ at $T = 0$ for $q_f = u, d$, in comparison with the lattice data in [54]. Here we take into account a 30% uncertainty, which corresponds to the order of subleading corrections in the large N_c expansion, on that the present NJL-model analysis has been based. This comparison would further constrain the parameter space (v, v_s) in Fig. 4 and the applicable size of the strong magnetic field strength: $1.2 \lesssim v \lesssim 1.5$, $v_s \lesssim 4$, in unit of GeV^{-2} , and $0.25 \lesssim eB_{\min} \lesssim 0.34$ in unit of GeV^2 . Thus too large v and v_s would drive $\Sigma_{u,d} < 1$, hence would be disfavored because of spoiling the magnetic catalysis at $T = 0$, which also places the lower bound on the strength of eB . This is due to too large destructive interference from the AMM contributions to the quark condensate. When this quantitative constraint is combined with the allowed regime in the phase diagram, Fig. 7, we see that the AIMC may necessarily take place at the same time the CIMC is present.

More precise eB and T dependence of the chiral and axial susceptibilities could be determined by fitting all the model parameters to available lattice data, as has been discussed in the literature [55] in light of the CIMC. Then one could more quantitatively discuss whether the AIMC can take place at the same time the chiral one does, though presence of the destructive interference would be obscure. This may be worth performing elsewhere.

- (iii) The AIMC may provide a hint to reveal whether in a sense of early thermomagnetic universe, the remnant of the $U(1)_A$ breaking in the origin of mass might be comparable with what the chiral breaking leaves, in contrast to the pure-thermal QCD in which the former might highly dominate [5].
- (iv) Confirmation of the AIMC by lattice QCD simulations for the AIMC at high temperatures might give evidence of the destructive chiral and axial breaking in the chiral and the axial susceptibilities, and effective chiral models without such destructive interference leading to both the CIMC and AIMC would be excluded.
- (v) Possible prospected studies along this AIMC also include correlation between the dual CIMC and AIMC and the topological susceptibility: as briefly aforementioned, in the case without magnetic fields, the susceptibility differences for the chiral and axial partners are firmly linked to the topological susceptibility, through the anomalous-chiral Ward identities [51–53], and can form what is called the QCD trilemma [49]. It would be noteworthy to look into the magnetic dependence on the topological

susceptibility, when a strong magnetic field is applied, and its sensitivity to the emergence of the chiral and axial inverse magnetic catalyses, through the chiral Ward identities.⁴

- (vi) Some cosmological implications to QCD axion coupled to thermomagnetic QCD could also be derived: if the topological susceptibility could drop faster around the chiral crossover regime, due to the strong magnetic field along with the CIMC and AIMC, the axion mass (with fixed axion decay constant) could also get smaller, implying a significant modification of estimate on the thermal relic abundance of axion as a dark matter candidate.
- (vii) Other possible application of the AIMC may be related to a stable neutral a_0 meson around the chiral crossover regime: note first that the susceptibilities scale with the associated meson masses like $\sim 1/m_{\text{mesons}}^2$, hence the degeneracy in the meson masses actually signals the (effective) restoration of the associated symmetry. Since we expect $m_{\pi^0} \simeq m_{(\delta^0=a_0^0)}$ due to the AIMC, the dominant decay channel $a_0^0 \rightarrow \pi^0 + \eta^0$ will almost be closed (no matter how the η^0 mass gets changed from the vacuum value around the chiral crossover regime), so that the neutral a_0 meson can be somewhat long lived. This might give phenomenological impact on meson physics relevant to heavy ion collision experiments.

Exploring those interesting issues are to be left, and pursued elsewhere.

ACKNOWLEDGMENTS

We are grateful to Heng-Tong Ding, Chowdhury Aminul Islam, Mamiya Kawaguchi, Sheng-Tai Li, Akio Tomiya, and Lang Yu for useful comments. This work was supported in part by the National Science Foundation of China (NSFC) under Grants No. 11747308, No. 11975108, No. 12047569, and the Seeds Funding of Jilin University (S. M.).

⁴In Ref. [56] a possible correlation between the CIMC and an IMC for the topological susceptibility has been discussed based on a different type of NJL-like description with 2 flavors, where the axial susceptibility like $\chi_{\pi-\delta}$ is not addressed, however. Note that the axial breaking, i.e., nonzero $\chi_{\pi-\delta}$ is not always equal to the topological susceptibility χ_{top} , as has recently been clarified in [49] by deeply studying the anomalous chiral-Ward identity. More precisely and rigorously, it involves the chiral breaking as well, and becomes equal to χ_{top} only when the chiral symmetry is completely restored (at $T \rightarrow \infty$). Therefore, the T dependence and quark mass dependence of $\chi_{\pi-\delta}$ cannot simply follow that of χ_{top} .

APPENDIX: USEFUL FORMULAS FOR POLARIZATION FUNCTIONS Π_π AND Π_δ

Substituting the quark propagator under the magnetic field in Eq. (5), which includes the AMM terms, into the polarization functions, we work on the Dirac trace quantities. For the pion polarization function in Eq. (13), we have

$$\begin{aligned} & \text{Tr}[\gamma_5 D_n(p_{\parallel}, p_{\perp}) F_n(p_{\parallel}, p_{\perp}) \gamma_5 D_m(p_{\parallel}, p_{\perp}) F_m(p_{\parallel}, p_{\perp})] \\ &= -8[f_1(n)f_1(m) - f_2^2 \cdot p_{\parallel}^2][(L_n L_m + L_{n-1} L_{m-1}) \cdot [p_{\parallel}^2 - (M_f^2 + \kappa_f^2 q_f^2 B^2)]] \\ & \quad - 2\text{sign}(q_f B) M_f \kappa_f q_f B (L_n L_m - L_{n-1} L_{m-1}) - 8p_{\perp}^2 L_{n-1}^1 L_{m-1}^1, \end{aligned} \quad (\text{A1})$$

where we have omitted the arguments for the generalized Laguerre polynomials, and defined

$$\begin{aligned} f_1(n) &\equiv p_{\parallel}^2 + (\kappa_f q_f B)^2 - M_f^2 - 2n|q_f B|, \\ f_2 &\equiv -2\kappa_f q_f B. \end{aligned} \quad (\text{A2})$$

In a similar way, for the delta meson polarization function in Eq. (15), we have

$$\begin{aligned} \text{Tr}[D_n(p_{\parallel}, p_{\perp}) F_n(p_{\parallel}, p_{\perp}) D_m(p_{\parallel}, p_{\perp}) F_m(p_{\parallel}, p_{\perp})] &= 8[f_1(n)f_1(m) + f_2^2 \cdot p_{\parallel}^2][(L_n L_m + L_{n-1} L_{m-1}) \cdot [p_{\parallel}^2 + (M_f^2 + \kappa_f^2 q_f^2 B^2)]] \\ & \quad + 2\text{sign}(q_f B) M_f \kappa_f q_f B (L_n L_m - L_{n-1} L_{m-1}) - 8p_{\perp}^2 L_{n-1}^1 L_{m-1}^1 \\ & \quad + 16(f_1(n) + f_1(m)) f_2 p_{\parallel}^2 M_f \text{sign}(q_f B) (L_n L_m - L_{n-1} L_{m-1}) \\ & \quad - 8p_{\parallel}^2 (f_1(n) + f_1(m)) f_2^2 (L_n L_m + L_{n-1} L_{m-1}), \end{aligned} \quad (\text{A3})$$

where

$$\begin{aligned} f_1(n) &= p_{\parallel}^2 + (\kappa_f q_f B)^2 - M_f^2 - 2n|q_f B|, \\ f_2 &= -2\kappa_f q_f B. \end{aligned} \quad (\text{A4})$$

Plugging those into Eq. (18) with Eqs. (11) and (14), and working on momentum integration with respect to p_{\perp} , and summing over Matsubara frequencies, we are then ready to evaluate the axial susceptibility numerically. Through this procedure, a couple of the results have been presented in the main text.

-
- | | |
|---|--|
| <p>[1] S. Aoki, H. Fukaya, and Y. Taniguchi, <i>Phys. Rev. D</i> 86, 114512 (2012).</p> <p>[2] T. Bhattacharya, M. I. Buchoff, N. H. Christ, H. T. Ding, R. Gupta, C. Jung, F. Karsch, Z. Lin, R. D. Mawhinney, G. McGlynn <i>et al.</i>, <i>Phys. Rev. Lett.</i> 113, 082001 (2014).</p> <p>[3] T. D. Cohen, <i>Phys. Rev. D</i> 54, R1867 (1996).</p> <p>[4] T. D. Cohen, <i>arXiv:nucl-th/9801061</i>.</p> <p>[5] S. Aoki, Y. Aoki, H. Fukaya, S. Hashimoto, C. Rohrhofer, and K. Suzuki (JLQCD Collaboration), <i>Prog. Theor. Exp. Phys.</i> 2022, 023B05 (2022).</p> <p>[6] T. Vachaspati, <i>Phys. Lett. B</i> 265, 258 (1991).</p> <p>[7] K. Enqvist and P. Olesen, <i>Phys. Lett. B</i> 319, 178 (1993).</p> <p>[8] D. Grasso and A. Riotto, <i>Phys. Lett. B</i> 418, 258 (1998).</p> <p>[9] D. Grasso and H. R. Rubinstein, <i>Phys. Rep.</i> 348, 163 (2001).</p> <p>[10] J. Ellis, M. Fairbairn, M. Lewicki, V. Vaskonen, and A. Wickens, <i>J. Cosmol. Astropart. Phys.</i> 09 (2019) 019.</p> | <p>[11] Y. Di, J. Wang, R. Zhou, L. Bian, R. G. Cai, and J. Liu, <i>Phys. Rev. Lett.</i> 126, 251102 (2021).</p> <p>[12] J. Yang and L. Bian, <i>arXiv:2102.01398</i>.</p> <p>[13] D. E. Kharzeev, L. D. McLerran, and H. J. Warringa, <i>Nucl. Phys. A</i> 803, 227 (2008).</p> <p>[14] V. Skokov, A. Y. Illarionov, and V. Toneev, <i>Int. J. Mod. Phys. A</i> 24, 5925 (2009).</p> <p>[15] W. T. Deng and X. G. Huang, <i>Phys. Rev. C</i> 85, 044907 (2012).</p> <p>[16] J. Błoczynski, X. G. Huang, X. Zhang, and J. Liao, <i>Nucl. Phys. A</i> 939, 85 (2015).</p> <p>[17] Y. Hirono, M. Hongo, and T. Hirano, <i>Phys. Rev. C</i> 90, 021903 (2014).</p> <p>[18] W. T. Deng and X. G. Huang, <i>Phys. Lett. B</i> 742, 296 (2015).</p> <p>[19] V. Voronyuk, V. D. Toneev, S. A. Voloshin, and W. Cassing, <i>Phys. Rev. C</i> 90, 064903 (2014).</p> <p>[20] X. G. Huang, <i>Rep. Prog. Phys.</i> 79, 076302 (2016).</p> <p>[21] M. D'Elia, <i>Lect. Notes Phys.</i> 871, 181 (2013).</p> |
|---|--|

- [22] G. Endrödi, Proc. Sci., LATTICE2014 (2014) 018 [arXiv:1410.8028].
- [23] V. G. Bornyakov, P. V. Buividovich, N. Cundy, O. A. Kochetkov, and A. Schäfer, Phys. Rev. D **90**, 034501 (2014).
- [24] G. S. Bali, F. Bruckmann, G. Endrödi, S. D. Katz, and A. Schäfer, J. High Energy Phys. **08** (2014) 177.
- [25] A. Tomiya, H. T. Ding, X. D. Wang, Y. Zhang, S. Mukherjee, and C. Schmidt, Proc. Sci., LATTICE2018 (2019) 163 [arXiv:1904.01276].
- [26] M. D'Elia, F. Manigrasso, F. Negro, and F. Sanfilippo, Phys. Rev. D **98**, 054509 (2018).
- [27] G. Endrodi, M. Giordano, S. D. Katz, T. G. Kovács, and F. Pittler, J. High Energy Phys. **07** (2019) 007.
- [28] G. S. Bali, F. Bruckmann, G. Endrodi, Z. Fodor, S. D. Katz, S. Krieg, A. Schafer, and K. K. Szabo, J. High Energy Phys. **02** (2012) 044.
- [29] M. Kobayashi and T. Maskawa, Prog. Theor. Phys. **44**, 1422 (1970).
- [30] M. Kobayashi, H. Kondo, and T. Maskawa, Prog. Theor. Phys. **45**, 1955 (1971).
- [31] G. 't Hooft, Phys. Rev. Lett. **37**, 8 (1976).
- [32] G. 't Hooft, Phys. Rev. D **14**, 3432 (1976); **18**, 2199(E) (1978).
- [33] E. J. Ferrer, V. de la Incera, and X. J. Wen, Phys. Rev. D **91**, 054006 (2015).
- [34] S. Fayazbakhsh and N. Sadooghi, Phys. Rev. D **90**, 105030 (2014).
- [35] N. Chaudhuri, S. Ghosh, S. Sarkar, and P. Roy, Phys. Rev. D **99**, 116025 (2019).
- [36] N. Chaudhuri, S. Ghosh, S. Sarkar, and P. Roy, Eur. Phys. J. A **56**, 213 (2020).
- [37] S. Ghosh, N. Chaudhuri, S. Sarkar, and P. Roy, Phys. Rev. D **101**, 096002 (2020).
- [38] K. Xu, J. Chao, and M. Huang, Phys. Rev. D **103**, 076015 (2021).
- [39] R. L. S. Farias, W. R. Tavares, R. M. Nunes, and S. S. Avancini, arXiv:2109.11112.
- [40] H. T. Ding, S. T. Li, S. Mukherjee, A. Tomiya, X. D. Wang, and Y. Zhang, Phys. Rev. Lett. **126**, 082001 (2021).
- [41] A. Tomiya, G. Cossu, S. Aoki, H. Fukaya, S. Hashimoto, T. Kaneko, and J. Noaki, Phys. Rev. D **96**, 034509 (2017).
- [42] P. Rehberg, S. P. Klevansky, and J. Hufner, Phys. Rev. C **53**, 410 (1996).
- [43] P. J. A. Bicudo, J. E. F. T. Ribeiro, and R. Fernandes, Phys. Rev. C **59**, 1107 (1999).
- [44] E. J. Ferrer and V. de la Incera, Phys. Rev. Lett. **102**, 050402 (2009).
- [45] E. J. Ferrer and V. de la Incera, Nucl. Phys. **B824**, 217 (2010).
- [46] L. Chang, Y. X. Liu, and C. D. Roberts, Phys. Rev. Lett. **106**, 072001 (2011).
- [47] E. J. Ferrer, V. de la Incera, I. Portillo, and M. Quiroz, Phys. Rev. D **89**, 085034 (2014).
- [48] S. Mao and D. H. Rischke, Phys. Lett. B **792**, 149 (2019).
- [49] C. X. Cui, J. Y. Li, S. Matsuzaki, M. Kawaguchi, and A. Tomiya, arXiv:2106.05674.
- [50] T. Hatsuda and T. Kunihiro, Phys. Rep. **247**, 221 (1994).
- [51] A. Gómez Nicola and J. Ruiz de Elvira, J. High Energy Phys. **03** (2016) 186.
- [52] A. Gomez Nicola and J. Ruiz de Elvira, Phys. Rev. D **97**, 074016 (2018).
- [53] M. Kawaguchi, S. Matsuzaki, and A. Tomiya, Phys. Rev. D **103**, 054034 (2021).
- [54] H. T. Ding, S. T. Li, A. Tomiya, X. D. Wang, and Y. Zhang, Phys. Rev. D **104**, 014505 (2021).
- [55] G. Endrödi and G. Markó, J. High Energy Phys. **08** (2019) 036.
- [56] M. S. Ali, C. A. Islam, and R. Sharma, Phys. Rev. D **104**, 114026 (2021).